This is an electronic reprint of the original article.
This reprint may differ from the original in pagination and typographic detail.

Aji, Arif; Hamuyuni, Joseph; Aromaa, Jari; Wilson, Benjamin P.; Lundström, Mari

Design of optimal electrolyte circulation based on the kinetic modelling of copper dissolution in silver electrorefining

Published in:
Hydrometallurgy

DOI:
10.1016/j.hydromet.2020.105403

Published: 01/09/2020

Document Version
Peer-reviewed accepted author manuscript, also known as Final accepted manuscript or Post-print

Published under the following license:
CC BY-NC-ND

Please cite the original version:
Aji, A., Hamuyuni, J., Aromaa, J., Wilson, B. P., & Lundström, M. (2020). Design of optimal electrolyte circulation based on the kinetic modelling of copper dissolution in silver electrorefining. *Hydrometallurgy*, *196*, Article 105403. https://doi.org/10.1016/j.hydromet.2020.105403

This material is protected by copyright and other intellectual property rights, and duplication or sale of all or part of any of the repository collections is not permitted, except that material may be duplicated by you for your research use or educational purposes in electronic or print form. You must obtain permission for any other use. Electronic or print copies may not be offered, whether for sale or otherwise to anyone who is not an authorised user.

Journal Pre-proof

Design of optimal electrolyte circulation based on the kinetic modelling of copper dissolution in silver electrorefining

Arif T. Aji, Joseph Hamuyuni, Jari Aromaa, Benjamin P. Wilson, Mari Lundström

PII: S0304-386X(19)31013-8

DOI: https://doi.org/10.1016/j.hydromet.2020.105403

Reference: HYDROM 105403

To appear in: *Hydrometallurgy*

Received date: 8 November 2019

Revised date: 1 May 2020

Accepted date: 17 June 2020

Please cite this article as: A.T. Aji, J. Hamuyuni, J. Aromaa, et al., Design of optimal electrolyte circulation based on the kinetic modelling of copper dissolution in silver electrorefining, *Hydrometallurgy* (2019), https://doi.org/10.1016/j.hydromet.2020.105403

This is a PDF file of an article that has undergone enhancements after acceptance, such as the addition of a cover page and metadata, and formatting for readability, but it is not yet the definitive version of record. This version will undergo additional copyediting, typesetting and review before it is published in its final form, but we are providing this version to give early visibility of the article. Please note that, during the production process, errors may be discovered which could affect the content, and all legal disclaimers that apply to the journal pertain.

© 2019 Published by Elsevier.

Design of optimal electrolyte circulation based on the kinetic modelling of copper dissolution in silver electrorefining

Arif T. Aji[1], Joseph Hamuyuni[2], Jari Aromaa[1], Benjamin P. Wilson[1], Mari Lundström[1*]
[1]School of Chemical Technology, Aalto University, PO Box 16200, FI-00076 AALTO, Finland
[2]Outotec (Finland) Oy, Research Center, Kuparitie 10, PO Box 69, FI-28101 Pori, Finland.
* corresponding author: mari.lundström@aalto.fi

Abstract

Copper is the major impurity dissolved in silver electrorefining which potentially accumulates in the electrolyte during the process and co-deposits onto the cathode surface, decreasing the product quality. The study investigated the dissolution kinetics of copper in silver electrorefining as a function of $wt\%_{Cu}$ in the industrial electrolyte ranges of 40 – 100 g/dm^3 $[Ag^+]$, 5 – 15 g/dm^3 $[HNO_3]$ and 20 – 60 g/dm^3 $[Cu^{2+}]$ at 25 – 45°C. The results showed that Cu dissolved at a higher rate in comparison to silver and that the two kinetic models developed have good accuracy and validity. From the models, optimal electrolyte circulation parameters were simulated to avoid $[Cu^{2+}]$ accumulation in the electrolyte. As a conclusion, processing 1% Cu anodes at the critical $[Cu^{2+}]/[Ag^+]$ ratio of 0.8 in the electrolyte requires an inlet of $[Ag^+]$ of 2.3 – 5.2 and tolerates $[Cu^{2+}]$ of 0.14 – 0.47 times that of the $[Ag^+]$ and $[Cu^{2+}]$ in the bulk electrolyte, respectively. Furthermore, electrolyte with higher $[Ag^+]$ provides the benefit of reduced electrolyte circulation flowrate and increased tolerance of $wt\%_{Cu}$ in the silver anodes.

Keywords: copper dissolution, model-based process design, silver electrorefining.

1. Introduction

Copper (Cu) is a common base metal impurity in the anodes of the silver (Ag) electrorefining process, either from primary sources [Habashi, 1997; Marsden and House, 2006] or various secondary sources [Balde et al. 2017]. Classic silver electrorefining uses a Moebius cell in $AgNO_3$ electrolyte with a silver concentration, $[Ag^+]$, of 30 to 200 g/dm^3, free acid concentration, $[HNO_3]$, of 0 to 10 g/dm^3 and operating temperature of 25 – 55°C [Mantell, 1940; Leigh, 1973; Cornelius, 1982; Pletcher and Walsh, 1990; Renner et al., 1993; Jaskula and Kammel, 1997; Pophanken and Friedrich, 2017]. The main silver anode compositions consist of silver, gold and copper with typical contents as shown in Table 1 [Mantell, 1940; Leigh, 1973; Cornelius, 1982; Pletcher and Walsh, 1990; Jaskula and Kammel, 1997; Pophanken and Friedrich, 2017].

Copper dissolution in a low concentration of nitric acid solution follows the reactions outlined in Eqs. (1-6) [Martinez et al. 1993; Ozmetin et al. 1998]. The overall reaction presented in Eq. (7) is based on a revised version published previously [Demir et al. 2004] and subsequently recalculated with HSC Chem 8.0 from Outotec.

Table 1. Typical Doré compositions.

Anode content	[Mantell, 1940]	[Cornelius, 1982]	[Leigh, 1973; Pletcher and Walsh, 1990]	[Jaskula and Kammel, 1997]	[Pophanken and Friedrich, 2017]
Ag (%)	85 – 99	98	86 – 92	99.3	96.5
Au (%)	0.01–15	0.5	8 – 9	0.04–0.07	0.01
Cu (%)	0.5 – 1	1	0.5 – 1	0.4 – 0.6	3

$$6Cu + 12HNO_3 \leftrightarrow 3Cu(NO_3)_2 + 3Cu(NO_2)_2 + 6H_2O \quad (1)$$

$$3Cu(NO_2)_2 + 6HNO_3 \leftrightarrow 3Cu(NO_3)_2 + 6HNO_2 \quad (2)$$

$$6Cu + 6HNO_3 + 6HNO_2 \leftrightarrow 6Cu(NO_2)_2 + 6H_2O \quad (3)$$

$$6Cu(NO_2)_2 + 12HNO_3 \leftrightarrow 6Cu(NO_3)_2 + 12HNO_2 \quad (4)$$

$$12HNO_2 + 12HNO_3 \leftrightarrow 24NO_2 + 12H_2O \quad (5)$$

$$24NO_2 + 8H_2O \leftrightarrow 16HNO_3 + 8NO \quad (6)$$

$$3Cu + 12HNO_3 \leftrightarrow 3Cu(NO_3)_2 + 4HNO_3 + 2NO + 4H_2O \quad (7)$$

Kinetic models of copper dissolution related to the effect of *[HNO₃]* and temperature proposed by Berg [Travnicek and Weber, 1960] are shown in Eq. (8-9) and a more recent model is detailed in Eq. (10) as derived from the results of Khodari et al. [Khodari et al., 2001].

$$r_{Berg\ 1}(g/cm^2 \cdot s^1) = 141 \cdot [HNO_3] \cdot (1-\alpha) \quad (8)$$

$$r_{Berg\ 2}(g/cm^2 \cdot s^1) = 1.33 \cdot T \cdot [HNO_3] \cdot (1-\alpha) \cdot exp(-8860/RT) \quad (9)$$

$$r_{Khodari\ et\ al.}\left(\frac{g}{cm^2} \cdot s^1, at\ 25°C\right) = 0.0056 \cdot [HNO_3] - 0.7035 \quad (10)$$

The increase of *[Cu^{2+}]* provides a benefit in the form of increased conductivity of the silver electrolyte [Aji et al. 2016]. Furthermore, with the lower standard potential of reduction, theoretically the presence of Cu should not affect the deposition process. Nevertheless, studies have found that Cu is co-deposited - which results in impurities within the Ag crystal product - at a certain level of *[Cu^{2+}]* in the electrolyte, and therefore the level of *[Cu^{2+}]* in the electrolyte needs to be limited [Leigh, 1973; Hunter, 1975; Pophanken and Friedrich, 2017; Pophanken and Friedrich, 2015]. While there are suggestions that co-deposition is either caused by the electrochemical deposition or mechanical inclusion of Cu salt into the Ag crystal product [Eger, 1924; Hunter, 1975; Prior, 1986; Renner et al., 1993; Haranczyk and Sedzimir, 1995;], several studies have concluded that to avoid Cu co-deposition, both the *[Cu^{2+}]* should be lower than that of *[Ag^{+}]* in the electrolyte (see Table 2) [Johnson, 1967; Leigh, 1973; Hunter, 1975; Pophanken and Friedrich, 2017;].

Journal Pre-proof

Table 2. $[Ag^+]$, $[HNO_3]$ and maximum $[Cu^{2+}]$ in silver electrolytes

Concentrations	[Johnson, 1967]	[Leigh, 1973]	[Hunter, 1975]	[Pophanken and Friedrich, 2017]	
$[Ag^+]$	40	150	60 – 160	65 – 120	> 60
$[HNO_3]$	0*	2 – 6.2*	0.2 – 2*	1 - 10	
$[Cu^{2+}]$	35	max 45	60	max 50 – 100	max 50–80
$[Cu^{2+}]/[Ag^+]$	0.875	0.3	0.5 – 1	0.77 – 0.83	0.8 – 1.3

* calculated from pH

The established concentration limitation of $[Cu^{2+}] < [Ag^+]$ results in the critical $[Cu^{2+}]/[Ag^+]$ ratios primarily within the range of 0.8 – 1. In this paper, we have studied the dissolution kinetics of pure copper in silver electrolyte by electrochemical methods. With the development knowledge related to Cu dissolution within the more complex parameters of silver electrorefining, $[Cu^{2+}]$ accumulation in the electrolyte and the quality of the product can be maintained even at higher current density operation. The objectives of this study are to develop a Cu dissolution kinetic model and design the optimal electrolyte circulation required to control the accumulation of $[Cu^{2+}]$ in the electrolyte.

2. Materials and Methods

Synthetic silver electrolyte parameters were selected in such a way as to simulate industrial silver electrorefining process conditions. $[Ag^+]$ range of 40 to 100 g/dm^3, $[HNO_3]$ between 5 to 15 g/dm^3 and a temperature range of 25 – 45°C (Table 3). The chemicals used were silver nitrate ($AgNO_3$, 99.8%, VWR Chemicals), copper nitrate ($Cu(NO_3)_2{\cdot}3H_2O$, 99%, VWR) and nitric acid (HNO_3, 65%, Merck).

Table 3. Experimental parameters and electrolyte concentrations investigated.

Factors	**Levels**	**Unit**
$[Ag^+]$	40; 70; 100	g/dm^3
$[Cu^{2+}]$	20; 40; 60	g/dm^3
$[HNO_3]$	5; 10; 15	g/dm^3
Temperature	25; 35; 45	°C

Copper electrodes of 99.99% grade were prepared by coating with an inert resin (Struers Aps, Denmark) and polished, so that only the cross-section of the electrode was exposed to the electrolyte bath. This freshly polished copper was then immersed into a 10% HNO_3 solution until the surface was

Journal Pre-proof

covered with a layer of evolved gas bubbles, before being subjected to cyclic voltammetry in order to ensure an oxide-free surface.

Voltammetry measurements were conducted with a Gill AC 1516 potentiostat (ACM Instruments, UK), with an Ag/AgCl (Mettler Toledo, USA) reference electrode and a platinum (99.999%, Kultakeskus Oy, Hämeenlinna, Finland) counter electrode with temperature control using a thermostatic MGW Lauda MT/M3 circulating water bath. Voltammetry measurements were conducted in reverse from 1000 to -100 mV vs. E_{corr} at a sweep rate of 50 mV/min and the design and analysis of experiments were conducted using Modde 8.0 (Umetrics, Sweden).

3. Theoretical Background

According to the phase diagram of Ag-Cu shown in Fig. 1, while silver and copper form a solid solution at high temperature, both metals tend to segregate at approximately 300°C in a slow cooling process. This segregation of Ag and Cu can result in the formation of copper or a copper-rich zones within silver anodes, which is the basic assumption of this paper.

Journal Pre-proof

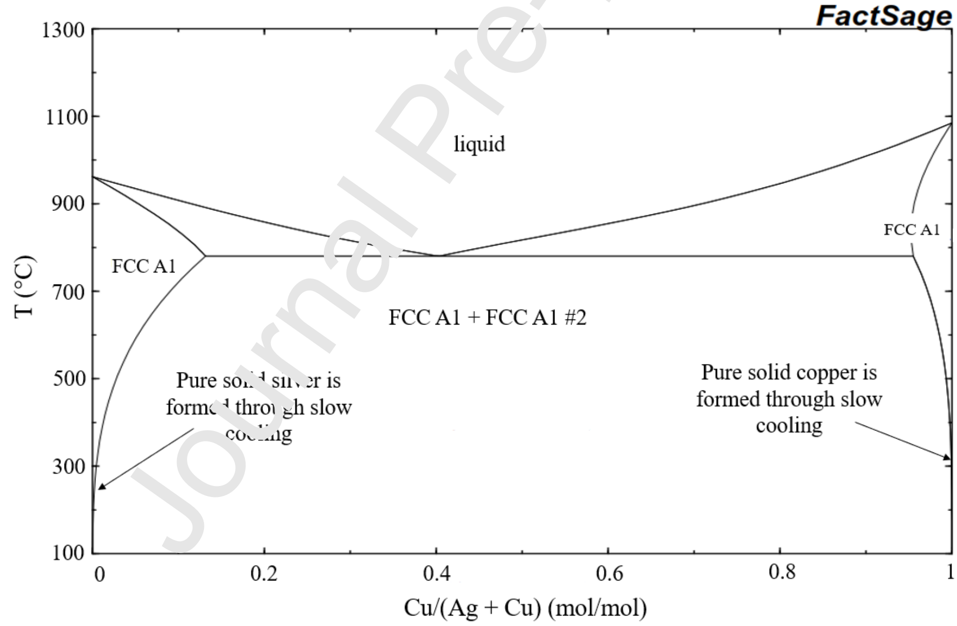

Fig. 1. Ag – Cu phase diagram showing that the pure metal phases are formed below 300°C [FactSage: SGnobl – SGTE noble metal alloy database 2010].

3.1. Kinetics modelling

Due to the presence of copper or copper-rich formations within silver anodes, the anodic current applied is used for the dissolution of both copper and silver. In contrast, the reaction on the cathode remains as silver reduction only, with reported current efficiencies > 92% [Mantell, 1940]. Consequently, these reactions result in the modification of $[Ag^{+}]$ and $[Cu^{2+}]$ during the electrorefining process as Cu is accumulated while Ag is depleted at specific rates determined by the partial current for Cu dissolution ($\hat{I}_{Cu}$). From the Faraday equation, for a cell volume (V_{cell}), the rate of $[Cu^{2+}]$ and $[Ag^{+}]$ can be expressed as follows in Eqs. (11-12):

$$d[Cu^{2+}]/_{dt}\,(\tfrac{g}{dm^3 s}) = +r_{[Cu^{2+}]} = \left(M_{Cu}/_{z_{Cu}F}\right)\cdot \hat{I}_{Cu}/_{V_{Cell}} \tag{11}$$

$$d[Ag^{+}]/_{dt}\left(\tfrac{g}{dm^3 s}\right) = -\,r_{[Ag^{+}]_{g/dm^3 s}} = \left(M_{Ag}/_{z_{Ag}F}\right)\cdot \hat{I}_{Cu}/_{V_{Cell}} \tag{12}$$

where $+r_{[Cu^{2+}]}$ and $-r_{[Ag^{+}]}$ are the accumulation and depletion rate of Cu and Ag in g/dm^3; M_{Ag} and M_{Cu} are the molecular mass of related metal; and z_{Cu} and z_{Ag} are the valences of copper and silver, respectively. From both equations, the correlation of $+r_{[Cu^{2+}]}$ and $-r_{[Ag^{+}]}$ can be written as in Eq. (13), which shows that the depletion rate of silver is more than triple that of the Cu dissolution rate:

$$-\,r_{[Ag^{+}]} = 3.39\cdot r_{[Cu^{2+}]} \tag{13}$$

To correlate Eq. (11) with current density, a modification was conducted through the introduction of the Cu phase surface area ($\hat{A}_{Cu}$) and anode surface area (A_a), as shown in Eq. (14). The form of Eq. (15) is taken as the kinetic model of Cu dissolution, with A_a/V_{ec} being the effective surface volume ratio of the total anode surface per litre of electrolyte. Moreover, although j_{Cu} modelling was conducted through a series of measurements, the $\hat{A}_{Cu}$ and A_a/V_{ec} values were based on industrial conditions.

Journal Pre-proof

$$r_{[Cu^{2+}]} = M_{Cu}/_{(z_{Cu}\cdot F)}\cdot\left(\hat{I}_{Cu}/_{A_{Cu}}\right)\cdot\left(A_{Cu}/_{A_a}\right)\cdot\left(A_a/_{V_{ec}}\right) \tag{14}$$

$$r_{[Cu^{2+}]} = M_{Cu}/_{(z_{Cu}\cdot F)}\cdot j_{Cu}\cdot \hat{A}_{Cu}\cdot\left(A_a/_{V_{ec}}\right) \tag{15}$$

3.2. Current density modelling

The empirical modelling of Cu dissolution current density was based on several models developed in a previous study [Khodari et al. 2001] and the logarithmic correlation [Aji et al. 2018] of each parameter. The proposed empirical models are outlined in Eqs. (16 – 19):

- Linear model (A)

$$j_{Cu} = C + m_{Ag}[Ag^{+}] + m_{Cu}[Cu^{2+}] + m_{HNO_3}[HNO_3] + m_T T \quad (16)$$

- Power model (B)

$$\log j_{Cu} = C + m_{Ag}[Ag^{+}] + m_{Cu}[Cu^{2+}] + m_{HNO_3}[HNO_3] + m_T T \quad (17)$$

- Concentration logarithmic (C)

$$\log j_{Cu} = C + m_{Ag}log[Ag^{+}] + m_{Cu}log[Cu^{2+}] + m_{HNO_3}log[HNO_3] + m_T T \quad (18)$$

- Full logarithmic (D)

$$\log j_{Cu} = C + m_{Ag}log[Ag^{+}] + m_{Cu}log[Cu^{2+}] + m_{HNO_3}log[HNO_3] + m_T log\, T \quad (19)$$

3.3. Copper surface fraction in the silver anode ($\hat{A}_{Cu}$)

With the assumption that particles are in the form of spheres, the radius after polishing (r_{cut}) has the Pythagoras relation with the initial radius (r) and height of cut (h_{cut}) expressed by Eq. (20), where r_{cut} is the radius of the exposed surface of the particle, r is the radius and h_{cut} is the height of the cut. Accordingly, the average r_{cut} of the sphere is shown by Eq. (21).

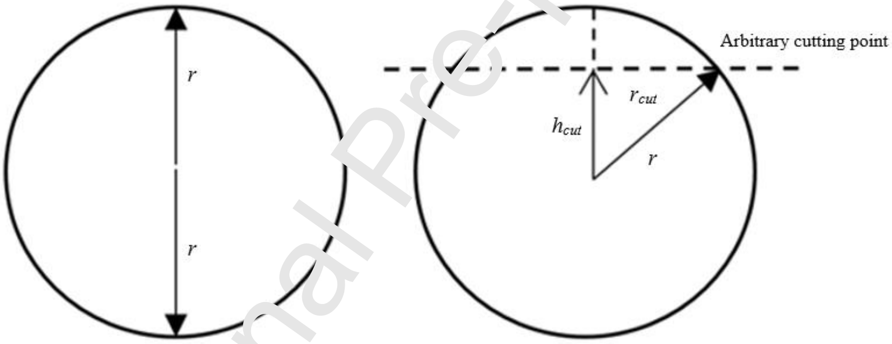

Fig. 2. Schematic of surface area partition of a spherical particle.

$$r_{cut} = \sqrt{r^2 - h_{cut}^2} \quad (20)$$

$$\overline{r}_{cut} = \frac{1}{n}\sum_{i=1}^{n} r_{cut} = \frac{1}{2r}\int_{-r}^{r}\left(\sqrt[2]{r^2 - h_{cut}^2}\right) dh \quad (21)$$

The average surface area can therefore be calculated based on the specific atom radius as in Eq. (22). Throughout the radius (-r to r), the average surface area for an i particle at any given section of the sphere is shown by Eq. (23).

$$\overline{A}_{cut} = \pi \cdot \overline{r}_{cut}^{2} = \pi \cdot \frac{1}{2r}\int_{-r}^{r}(r^2 - h_{cut}^2)dh \quad (22)$$

$$\overline{A}_{cut,i} = \frac{2}{3}\pi \cdot r_i^2 \quad (23)$$

Journal Pre-proof

As the major constituents of silver anodes are Ag-Au-Cu, as shown in Table 1, the total electrode surface can be assumed to be the sum of these metal surface fractions, see Eq. (24). With the known radius and molecular weight of the metals, the Cu surface fraction ($\hat{A}_{Cu}$) can be calculated using Eq. (25):

$$\hat{A}_{Cu} = {}^{A_{Cu}}\!/_{A_{total}} = {}^{N_{Cu} \cdot \bar{A}_{Cu}}\!/_{\left(N_{Ag} \cdot \bar{A}_{Ag} + N_{Au} \cdot \bar{A}_{Au} + N_{Cu} \cdot \bar{A}_{Cu}\right)} \tag{24}$$

$$\hat{A}_{Cu} = {}^{wt\%_{Cu}}\!/_{\left(0.74 \cdot wt\%_{Ag} + 0.41 \cdot wt\%_{Au} + wt\%_{Cu}\right)} \tag{25}$$

3.4. Active surface per volume of electrolyte (${}^{A_a}\!/_{V_{ec}}$)

For the variable of A_a/V_{ec}, values were determined from different industrial silver anode sizes and cell geometries as shown in Table 4, with the ratios of anode active surface to volume of electrolyte in the range of 0.003 – 0.005 m^2/dm^3.

Table 4. Geometrical data of Moebius Cells for the calculation of A_a/V_{ec}

Parameters	[Mantell, 1940]			
	USA 1	Canada	Germany	USA 2
A_{anode} (m^2)	1.13	1.05	0.80	1.08
V_{ec} (dm^3)	207	357	250	239
${}^{A_a}\!/_{V_{ec}}$	0.005	0.003	0.003	0.004

4. Results and Discussion

The current density operation of silver electrorefining can be divided into a moderate current density of 200–600 A/m^2 and high current density of 600–1000 A/m^2 [Aji et al. 2018]. High current density operation is ideally at 200–[illegible]00 mV vs. $E_{corr,Ag}$ or in the range of 625–725 mV vs. Ag/AgCl [Aji et al. 2018]. In addition, the presence of gold suggests that the optimal potential range is between 700–720 mV vs. Ag/AgCl [Aji et al. 2019]. Currently, high current density silver electrorefining is the industrial standard utilized for modern silver electrorefining, with at least 11 units installed by 2014 [Maliarik, 2014]. As a result, a series of anode polarization curves were measured (some examples are displayed in Fig. 3) and the related average current density values, at the selected range of 700–720 mV vs. Ag/AgCl, are shown in Table 5.

Journal Pre-proof

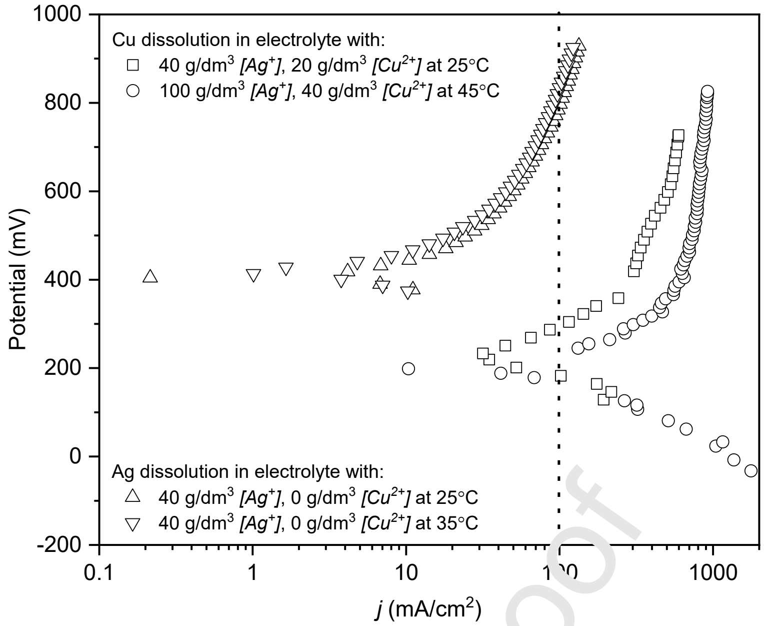

Fig. 3. Potentiodynamic measurements of Cu and Ag under various electrolyte conditions.

Table 5. Current density within the range of 700 - 720 mV vs. Ag/AgCl for Cu

[Ag$^+$] (g/dm^3)	*[Cu^{2+}]* (g/dm^3)	*[HNO$_3$]* (g/dm^3)	Temperature (°C)	Average current density at 700 - 720 mV vs Ag/AgCl (A/m^2)
40	20	5	25	5859 ± 59
40	40	10	35	6786 ± 142
40	60	15	45	7698 ± 47
70	20	10	45	7270 ± 45
70	40	15	25	6916 ± 59
70	60	5	35	7745 ± 60
100	20	15	35	8306 ± 100
100	40	5	45	8682 ± 75
100	60	10	25	6995 ± 39
70	40	10	35	7966 ± 90
70	40	10	35	8110 ± 2
70	40	10	35	7998 ± 87

4.1. Kinetic modelling of copper dissolution

The current density values from Table 5 were plotted with the calculated values from models A – D as shown in Eqs. (16 – 19). With the requirements defined for a good model as R^2 and $Q^2 > 0.5$, validity > 0.25 and reproducibility close to 1 [Eriksen et al. 2008], it was found that model C was clearly the best model, whereas model B failed due to the low validity value (Fig. 4).

Journal Pre-proof

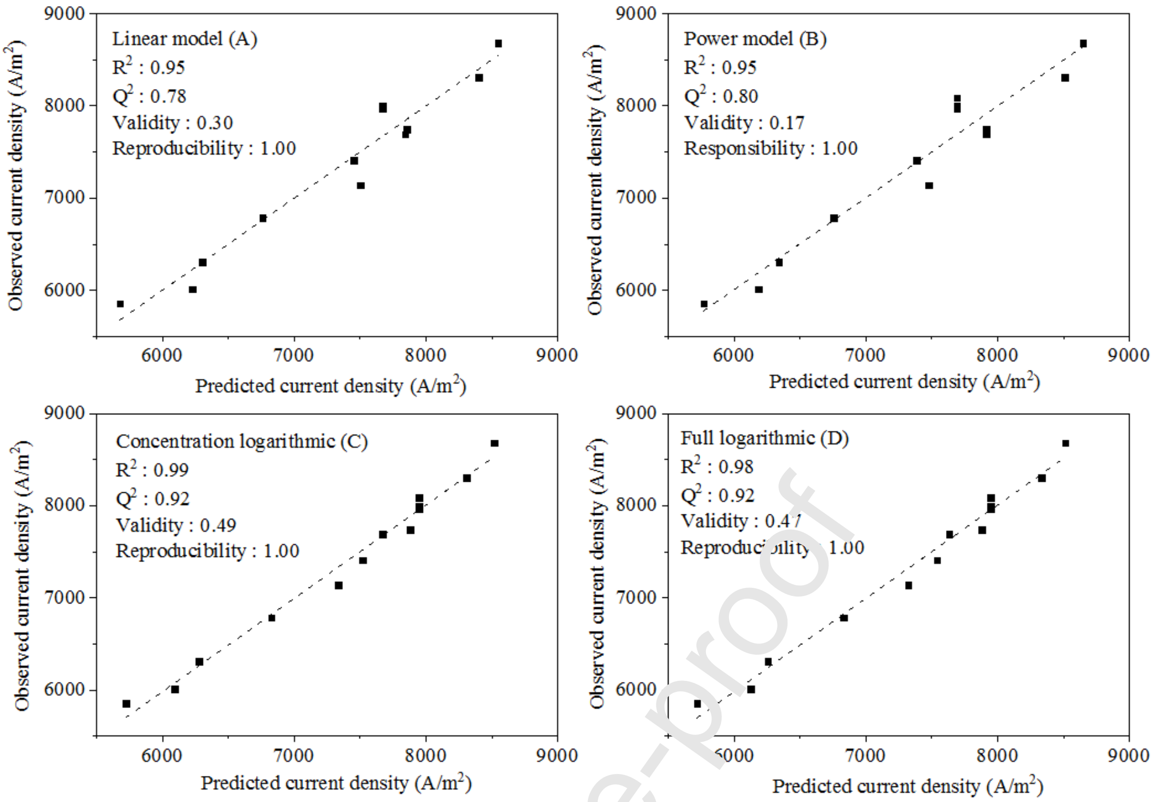

Fig. 4. Predicted and measured values of current density from models A, B, C and D.

The concentration logarithmic model C is also in agreement with the Ag dissolution model of a previous study [Aji et al. 2018]. Nevertheless, as $[Cu^{2+}]$ is absent in the fresh electrolyte, therefore the model is only valid throughout the range of concentration of this study. On the other hand, although the linear model has lower validity, the model still qualifies as a good model under the set criteria and therefore can be used for zero values of $[Cu^{2+}]$. In contrast, the full logarithmic model (model D) – which contains the additional temperature function in comparison to model C - was determined to be slightly inferior to the concentration logarithmic model (model C). Based on the modelling results, linear and concentration logarithmic models are suggested with the proviso that the concentration logarithmic model (A) is only valid for $[Cu^{2+}]$ in a range between 20 – 60 g/dm^3. Further analysis of the related scaled and centred coefficient value parameters for the models – as shown in Fig. 5 – both models can be expressed as in Eqs. (26 and 27).

Journal Pre-proof

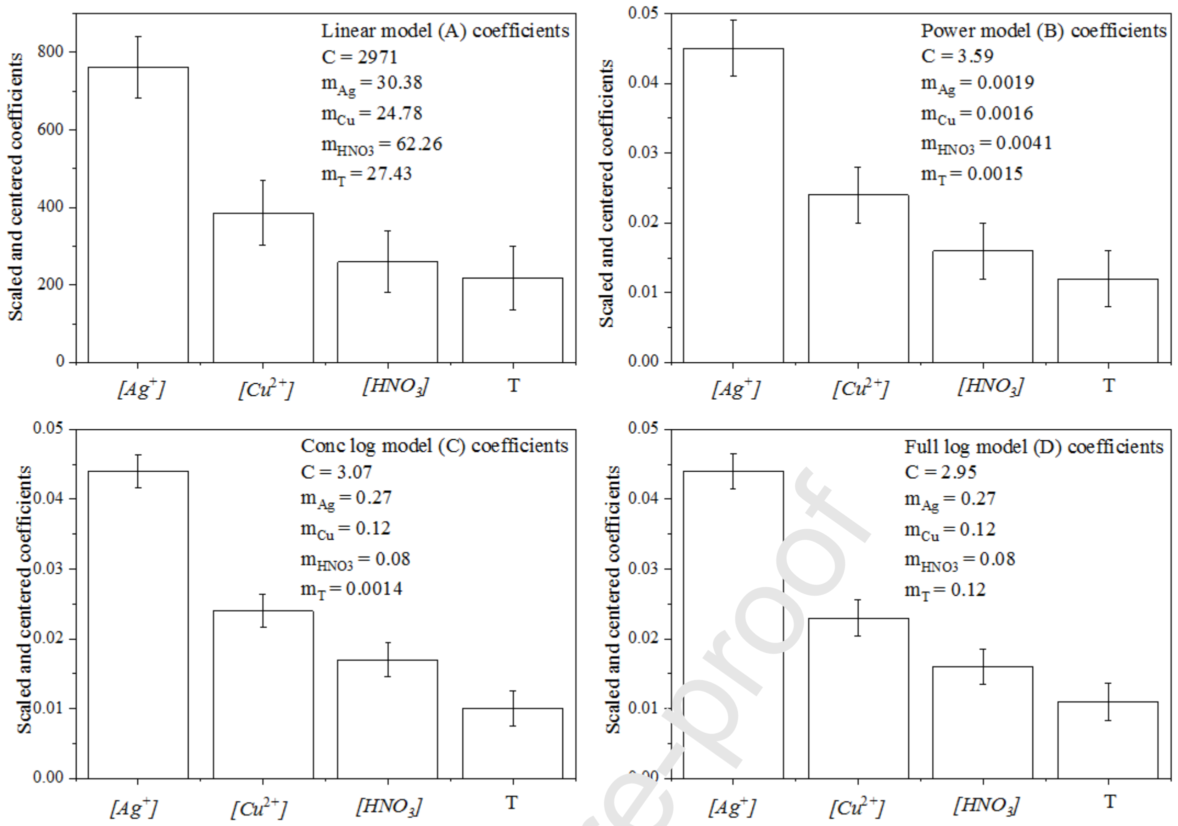

Fig. 5. Scaled and centred coefficient value parameters of models A, B, C and D.

$$\log j_{Cu} = 3.07 + 0.27\log[Ag^{+}] + 0.12\log[Cu^{2+}] + 0.08\log[HNO_3] + 0.0014T \qquad (26)$$

$$j_{Cu} = 2971 + 30.38[Ag^{+}] + 24.78[Cu^{2+}] + 62.26[HNO_3] + 27.43T \qquad (27)$$

As can be seen from Fig. 6, at the investigated elevated potential applied, the previous model outlined by Berg (see Eq. 9) is unable to accurately calculate the related kinetics when compared to the new models in this study. While the overpotential was the obvious reason for the Berg model inaccuracy, the additional variables utilized like *$[Ag^{+}]$* and *$[Cu^{2+}]$* also had a substantial impact.

Journal Pre-proof

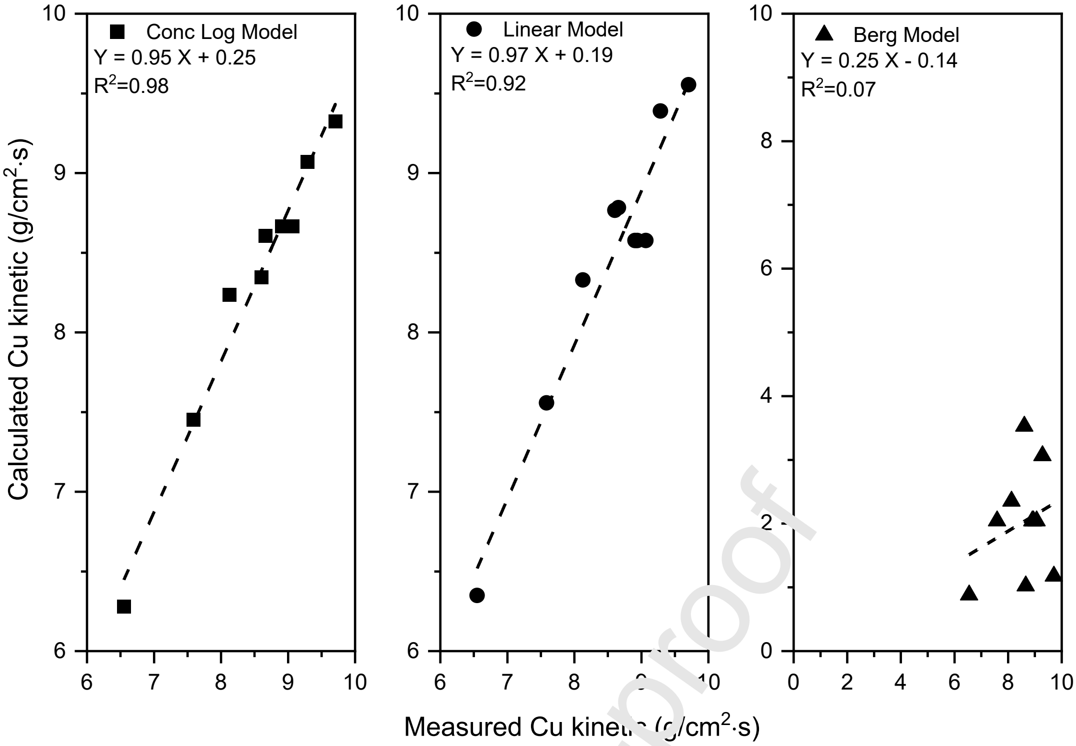

Fig 6. Comparison of Concentration Logarithmic, Linear and Berg models

4.2. Electrolyte circulation and treatment

Electrolyte circulation is conducted to maintain a constant level of $[Ag^+]$, $[HNO_3]$ and T in the bulk electrolyte. A certain flowrate of the electrolyte is circulated through a discharge (outflow) and the introduction of make-up electrolyte (inflow), as shown in Fig. 7. The discharged electrolyte goes to $[Cu^{2+}]$ removal and is then mixed with fresh $AgNO_3$ to improve the $[Ag^+]$ level before being circulated back to the process [Abrahamian, 2016; Virolainen, 2019].

Journal Pre-proof

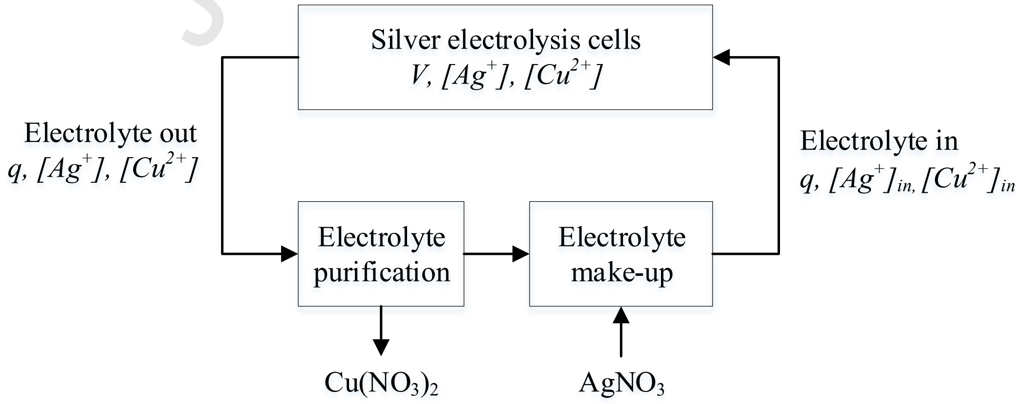

Fig 7. Schematic of closed-loop electrolyte circulation in a silver electrorefining process.

Through purification and mixing, the inlet electrolyte composition has a certain composition of remaining $[Cu^{2+}]$ and high $[Ag^{+}]$. The ratio of $[Cu^{2+}]$ and $[Ag^{+}]$ of the inlet electrolyte to the bulk electrolyte can be written according to the general form of Eq. (28) where M is Ag or Cu. With constant values of $[Ag^{+}]$, $[HNO_3]$ and T due to the electrolyte circulation, the models in Eqs. (26 – 27) can be simplified to Eq. (30) for the concentration logarithmic (model C) and Eq. (31) for the linear model (model A). Consequently, the models are defined as functions of $[Ag^{+}]$ and $[Cu^{2+}/Ag^{+}]$ in the electrolyte with α and β as the constants from the effect of other variables. Therefore, the calculated accumulation rate of $[Cu^{2+}]$ (r_{Cu}, g/dm^3·hour) in the electrolyte at different levels of $[Ag^{+}]$ and $[Cu^{2+}/Ag^{+}]$ can be determined as shown in Fig. 8.

$$\varepsilon_M = {[M^{n+}]_{in}}/{[M^{n+}]} \tag{28}$$

$$\log j_{Cu} = \alpha + 0.12 \cdot \log {[Cu^{2+}]}/{[Ag^{+}]} + 0.12 \cdot \log[Ag^{+} \tag{29}$$

$$j_{Cu} = \beta + 24.78[Ag^{+}]\left({[Cu^{2+}]}/{[Ag^{+}]} \right) \tag{30}$$

Journal Pre-proof

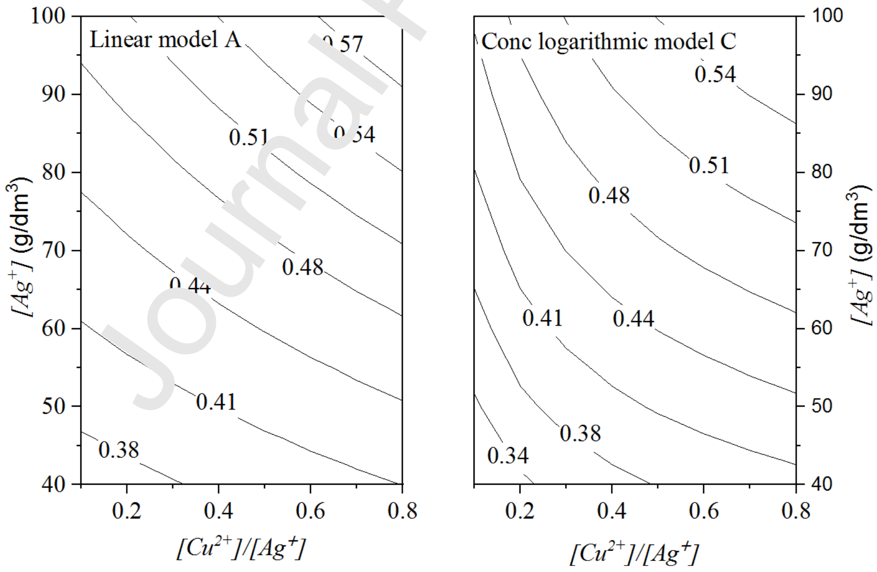

Fig. 8. Contour map of r_{Cu2+} (g/dm^3·hour) of models A and C for an anode containing 1% Cu and 5% Au as a function of $[Cu^{2+}/[Ag^{+}]$ and $[Ag^{+}]$.

Recently published purification methods are copper hydrolysis [Aprahamian, 2016] and ion exchange [Virolainen, 2019]. The first-mentioned process has claimed a 53 – 86% removal rate of Cu content from the bleed electrolyte. This process was run with an initial electrolyte of 81 g/dm^3 of $[Ag^{+}]$ and 66.4 g/dm^3 of $[Cu^{2+}]$ [Aprahamian, 2016]. Meanwhile, the second process was able to remove 78% of Cu from electrolyte containing 84 g/dm^3 $[Ag^+]$ and 41 g/dm^3 $[Cu^{2+}]$ and produces a final solution with $[Cu^{2+}]$ of 10 g/dm^3 [Virolainen, 2019]. With these Cu removal rates, in a closed-loop system, the inlet to bulk ratio of $[Cu^{2+}]$ as defined by Eq. (28) has a value within the range of 0.14 – 0.47.

4.3. Effect of *[Ag⁺]* and *[Cu²⁺]* in electrolyte circulation

By using a mixed flow reactor assumption [Levenspiel, 1999] and constant $[Ag^+]$, the balance of $[Ag^+]$ due to the electrolyte circulation can be determined via Eq. (31). Further combination of Eq. (31) with the definitions of $r_{[Ag^+]}$ in Eq. (14) and ε_M in Eq. (29) results in Eq. (32), which allows the required flowrate (q/V) to maintain $[Ag^+]$ to be calculated.

$$0 = r_{[Ag^+]} + {}^{q}/_{V} \cdot [Ag^+]_{in} - {}^{q}/_{V} \cdot [Ag^+] \tag{31}$$

$$ {}^{q}/_{V} = 3.39 \cdot r_{[Cu^{2+}]} \cdot {}^{1}/_{[Ag^+]} \cdot {}^{1}/_{(\varepsilon_{Ag} - 1)} \tag{32}$$

Similarly, the balance of Cu can be written as Eq. (34) for a constant $[Cu^{2+}]$ in the electrolyte. By substituting the value of q/V from Eq. (32), the equation can be written into Eq. (34). The equation gives information on the quality of the inlet electrolyte (ε_{Ag} and ε_{Cu}) based on the concentration ratio of $[Cu^{2+}]/[Ag^+]$ of the electrolyte to avoid copper accumulation.

$$0 = r_{[Cu^{2+}]} + {}^{q}/_{V} \cdot [Cu^{2+}] \cdot (\varepsilon_{Cu} - 1) \tag{33}$$

$$(\varepsilon_{Ag} - 1) = 3.39 \cdot {}^{[Cu^{2+}]}/_{[Ag^+]} \cdot (1 - \varepsilon_{Cu}) \tag{34}$$

At a critical $[Cu^{2+}]/[Ag^+]$ ratio of 0.8, Eq. 34 can be further simplified to Eq. (35):

$$\varepsilon_{Ag} = 3.7 - 2.7 \cdot \varepsilon_{Cu} \tag{35}$$

With the ε_{Cu} values of 0.14 – 0.47 from the purification process [Virolainen, 2019], according to Eq. (35) the suggested $[Ag^+]_{in}$ is in the range of 2.4 – 3.3 times that of the $[Ag^+]$ in the bulk electrolyte. As an example, the $[Ag^+]_{in}$ for 100 g/dm^3 $[Ag^+]$ bulk electrolyte ranges from 240 – 330 g/dm^3. When the concentrations of inlet electrolyte in terms of ε_{Cu} (0.14 – 0.47) and ε_{Ag} (2.4 – 3.3) are known, calculation of the flowrate as the final parameter of electrolyte circulation was simulated by using the linear current density model. The models established in this study were utilized in the design of an

Journal Pre-proof

ideal electrolyte circulation for different electrolyte conditions. Following the process schematic shown in Fig. 7, the contour diagrams of the calculated circulation flowrates per 100 dm^3 bulk volume based on anodes with 1% Cu and 5% Au content, 5 g/dm^3 $[HNO_3]$ and a temperature of 35°C for different types of electrolytes are shown in Fig. 9.

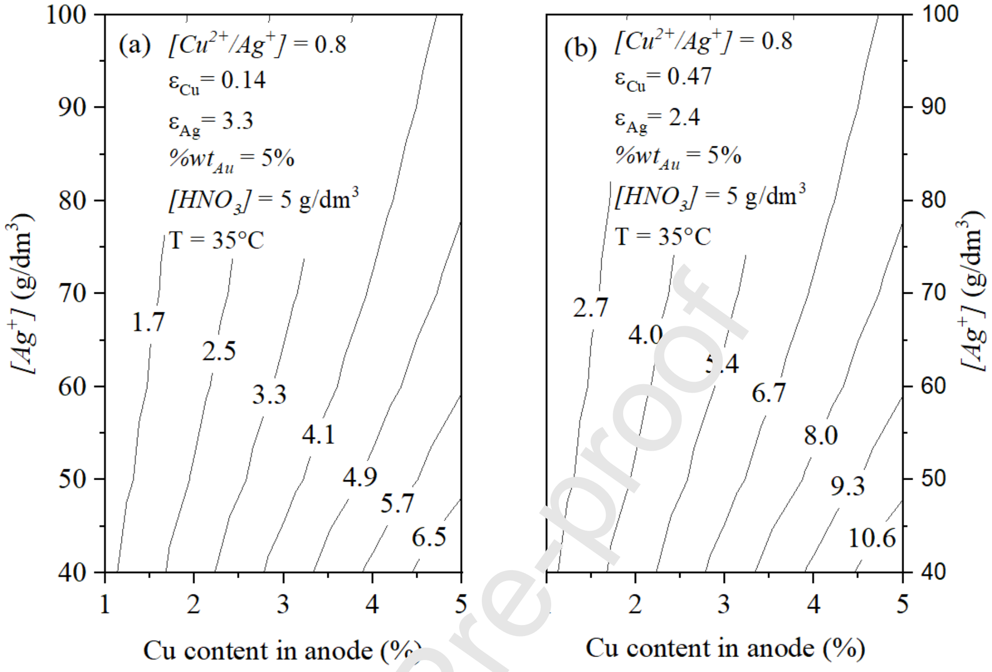

Fig. 9. Electrolyte circulation flowrate per 100 dm^3 bulk electrolyte for 1% Cu content in the anode at critical $[Cu^{2+}]/[Ag^{+}]$ ratios as a function of $\%wt_{Cu}$ and $[Ag^{+}]$.

Fig. 9 shows the optimal design of circulation flowrate, with figure 9 (a) showing the flowrate for low ε_{Cu} while the right-hand figure shows the circulation for high ε_{Cu}. As can be seen, the lower ε_{Cu} condition resulted in lower flowrate circulation. In addition, higher $[Ag^{+}]$ content electrolyte also resulted in a lower flowrate to replenish the $[Ag^{+}]$ in the bulk electrolyte. This study shows that the accumulation of $[Cu^{2+}]$ in the electrolyte due to the dissolution of the Cu in the silver anode can be avoided by optimizing the electrolyte circulation. Nevertheless, although further economic assessment is required, optimization of electrolyte circulation can provide the process with a higher tolerance to anode impurity.

5. **Conclusions**

The presence of copper in silver anodes as the major dissolved impurity in silver electrorefining poses a challenge due to the co-deposition of Cu in the silver crystal product, thus reducing the product quality. While copper is easily and rapidly dissolved, the large difference in reduction potential between copper and silver allows operation even at a $[Cu^{2+}]/[Ag^{+}]$ ratio as high as 0.8 without the co-deposition of copper on the cathode. Furthermore, $[Cu^{2+}]$ improves electrolyte conductivity thus

Journal Pre-proof

providing an economic benefit in the lower cell potential of the operation. From simulations of several electrolyte conditions, it is now known that only a small volume of electrolyte circulation is required in a closed loop process to maintain the level of *[Ag$^+$]* and *[Cu^{2+}]* in the electrolyte. Consequently, the economic refining of high Cu content silver anodes to produce a high purity final product is theoretically possible.

Acknowledgments

This research was carried out using facilities provided by the Academy of Finland's RawMatTERS Finland Infrastructure (RAMI-FIRI) at Aalto University. In addition, Arif T. Aji would like to acknowledge the funding support from LPDP (Indonesian Endowment Fund for Education), and Business Finland funded projects Circular Metal Ecosystem (CMEco) and Symmet.

References

1. F. Habashi, Precious Metals. Handbook of Extractive Metallurgy, vol III., Weinheim, New York, 1997, pp. 1215-1267.
2. J. Marsden, I. House, Refining. Chemistry of Gold Extraction Society for Mining, Metallurgy and Exploration Inc: Colorado, USA, 2006, pp. 451-4[illegible]3.
3. C. P. Balde, V. Forti, V. Gray, R. Kuehr, P. Stegmann, The Global E-waste Monitor 2017, United Nations University: Tokyo, 2017.
4. C. L. Mantell, Industrial Electrochemistry, McGraw-Hill, 1940, pp. 253-254.
5. A. H. Leigh, Precious metals refining practice. In 2nd International Symposium on Hydrometallurgy, 1973, pp. 95-[illegible]10.
6. G. Cornelius, Die Raffination von Gold und Silber durch Elektrolyse. In Elektrolyse der Nichteisenmetalle: 11. Metallurgisches Seminar, 1982, pp. 215 – 226.
7. D. Pletcher, F. C. Walsh, Industrial Electrochemistry, Chapman and Hall, London, 1990.
8. H. Renner, G. Schlamp, K. Zimmermann, W. Weise, P. Tews, K. Dermann, A. Knödler, K. H. Schröder, B. Kempf, H. M. Lüschow, and R. Drieselmann, Silver, silver compounds, and silver alloys, Ullmann's Encyclopedia of Industrial Chemistry, 1993.
9. M. Jaskula, R. Kammel, Unterschingen zur verbesserung des platinmetalausbringens bei der industriellen silberraffination. Metall 1997, 51, pp. 393 - 400.
10. A. K. Pophanken, B. Friedrich, Challenges in the electrolytic refining of silver - influencing the co-deposition through parameter control. Rare Metal Technology, 2017, pp. 327-380.
11. E. A. Travnicek, and J. H. Weber, Continuous dissolution of copper by nitric acid, The Journal of Physical Chemistry 65, no. 2, 1961, pp. 235-240.
12. Khodari, M., Abou-Krisha, M.M., Assaf, F.H., El-Cheikh, F.M. and Hussien, A.A., 2001. Stripping voltammetric and conductance measurements on corrosion and inhibition of copper in nitric acid. Materials chemistry and physics, 71(3), pp.279-290.

Journal Pre-proof

13. A. T. Aji, T. Kalliomäki, B. P. Wilson, J. Aromaa, M. Lundström, Modelling the effect of temperature and free acid, silver, copper and lead concentrations on silver electrorefining electrolyte conductivity, Hydrometallurgy, 2016, 166, pp. 154-159.
14. A. Pophanken, B. Friedrich, Influence of Electrolysis Parameter on the Co-Deposition of Impurities during Silver Electrorefining, EMC, 2015.
15. W. Hunter, Electrolytic refining, United States patent, 1975.
16. A. Prior, Elektrolytisches Silberraffinationsverfahren, 0 214 116 A1, 1986.
17. I. Haranczyk, J. Sedzimir, Copper and lead in the electrorefining of silver and their recovery from the waste solution, archives metallurgy, 40, 1995, 3, pp. 285 – 295.
18. G. Eger, Fortschritte in der Scheidung edelmetallhaltiger Legierungen, Zeitschrift für angewandte Chemie, 37, 1924, 11, pp. 137–144.
19. O. Johnson, Chapter 5 - Refining Processes, in Silver: Economics, Metallurgy, and Use, Butts, A; Coxe, C. D., D. Van Nostrand Company, Inc., Princeton, New Jersey, 1967.
20. A. Aji, S. Purwadaria, J. Aromaa, B. P. Wilson, O. Forsen, M. Lundström, The effect of gold on anode passivation and high current density operation under simulated silver electrorefining conditions, Hydrometallurgy, 2016, vol. 166, pp. 57–61.
21. A. T. Aji, J. Aromaa, B. P. Wilson, U. S. Mohanty, M. Lundström, Kinetic Study and Modelling of Silver Dissolution in Synthetic Industrial Silver Electrolyte as a Function of Electrolyte Composition and Temperature, Corrosion Science, 2018, pp. 163 – 169.
22. A. T. Aji, P. Halli, A. Guimont, B. P. Wilson, J. Aromaa, & M. Lundström, Modelling of silver anode dissolution and the effect on gold as impurity under simulated industrial silver electrorefining conditions. Hydrometallurgy, 2019, vol 189, 105105.
23. M. Maliarik, High current density silver electrorefining process: technology, equipment, automation and Outotec's Silver Refinery Plants. Hydrometallurgy: Proceedings of the 7th International Symposium, 2014, Vol. 2.
24. L. Eriksson, E. Johansson, N. Kettaneh-Wold, C. Wikström, S. Wold, Design of Experiments, Umetrics Academy, 2008, pp 78
25. V. Aprahamian, M. Tangen, G. B. Harris, C. W. White, Royal Canadian Mint silver electrorefining bleed treatment, IMPC 2016: XXVIII International Mineral Processing Congress, Canadian Institute of Mining, Metallurgy and Petroleum, Quebec City, Canada; 2016.
26. S. Virolainen, O. Holopainen, M. Maliarik, & T. Sainio, T, Ion exchange purification of a silver nitrate electrolyte. Minerals Engineering, 2019, vol 132, 175-182.
27. O. Levenspiel., Chemical reaction engineering, John Wiley and Sons, 1999.

Journal Pre-proof

Conflicts of Interest: The authors declare no conflict of interest.

Journal Pre-proof

Arif. T. Aji was responsible of the conceptualization, design of experiments and performed the experimental work, Joseph Hamuyuni supported on the thermodynamics analysis and design of experiments, B.P.W provided critical and constructive comments during the manuscript writing and reviewing, all the works was conducted under supervision of Jari Aromaa and Mari Lundström.

Journal Pre-proof

Highlights

- Valid and accurate models for Cu dissolution kinetics in Ag ER were built
- Optimal electrolyte circulation parameters were simulated to avoid Cu accumulation
- Inlet optimum: *[Ag^{+}]* 2.3 – 3.3 and *[Cu^{2+}]* 0.14-0.47 times of the bulk concentration
- Low flowrate, app. 10 dm^3/h, is required for every 100 dm^3 bulk electrolyte volume.

Journal Pre-proof

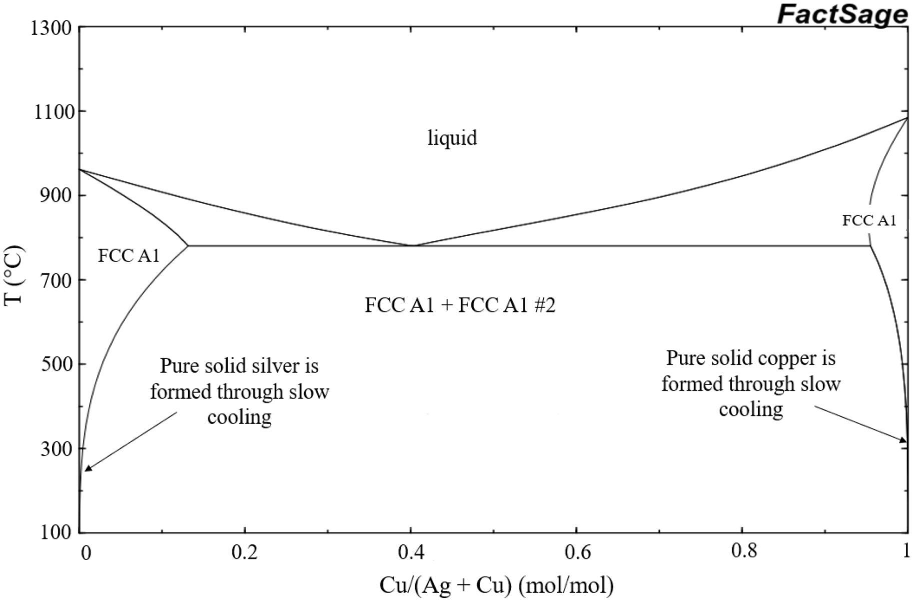
FactSage
1300
1100
900
700
500
300
100
T (°C)
0
0.2
0.4
0.6
0.8
1
Cu/(Ag + Cu) (mol/mol)
liquid
FCC A1
FCC A1
FCC A1 + FCC A1 #2
Pure solid silver is formed through slow cooling
Pure solid copper is formed through slow cooling

Figure 1

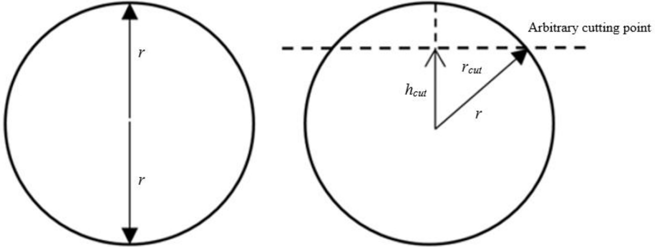

Figure 2

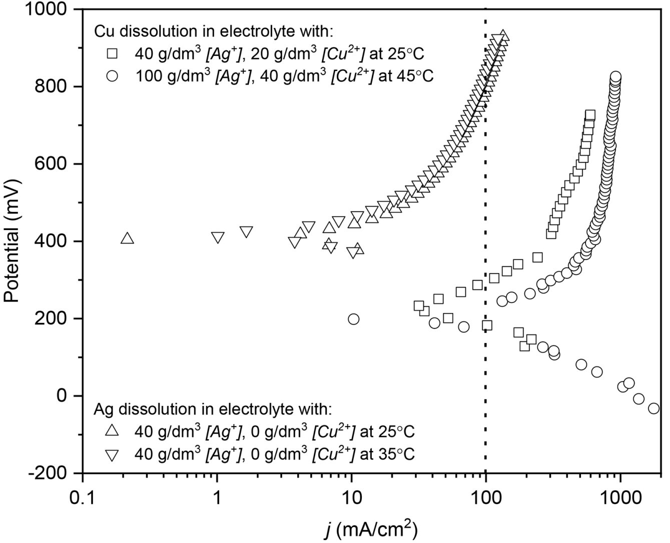

Cu dissolution in electrolyte with:
□ 40 g/dm3 [Ag+], 20 g/dm3 [Cu2+] at 25°C
○ 100 g/dm3 [Ag+], 40 g/dm3 [Cu2+] at 45°C
Ag dissolution in electrolyte with:
△ 40 g/dm3 [Ag+], 0 g/dm3 [Cu2+] at 25°C
▽ 40 g/dm3 [Ag+], 0 g/dm3 [Cu2+] at 35°C
Potential (mV)
1000
800
600
400
200
0
-200
0.1
1
10
100
1000
j (mA/cm2)

Figure 3

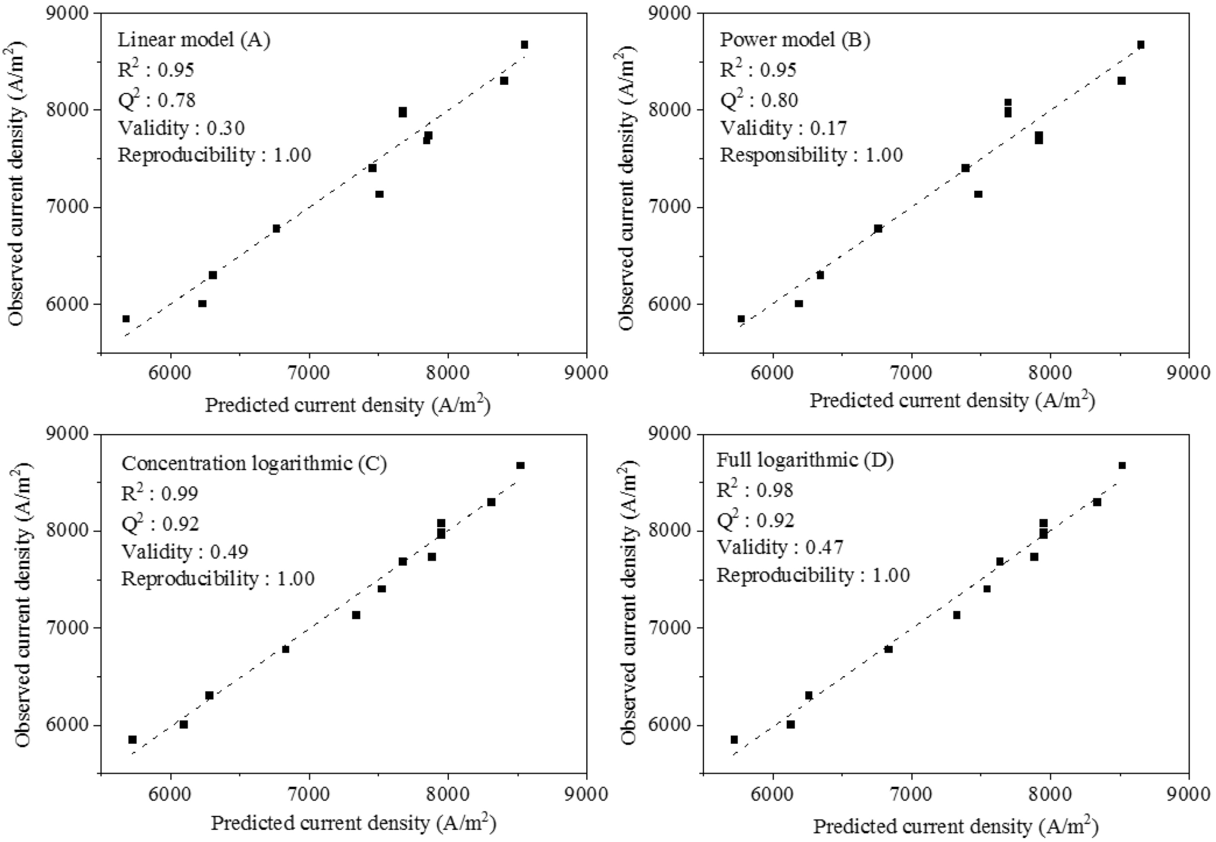
Linear model (A)
R^2 : 0.95
Q^2 : 0.78
Validity : 0.30
Reproducibility : 1.00
Power model (B)
R^2 : 0.95
Q^2 : 0.80
Validity : 0.17
Responsibility : 1.00
Concentration logarithmic (C)
R^2 : 0.99
Q^2 : 0.92
Validity : 0.49
Reproducibility : 1.00
Full logarithmic (D)
R^2 : 0.98
Q^2 : 0.92
Validity : 0.47
Reproducibility : 1.00
Observed current density (A/m^2)
Predicted current density (A/m^2)
6000
7000
8000
9000

Figure 4

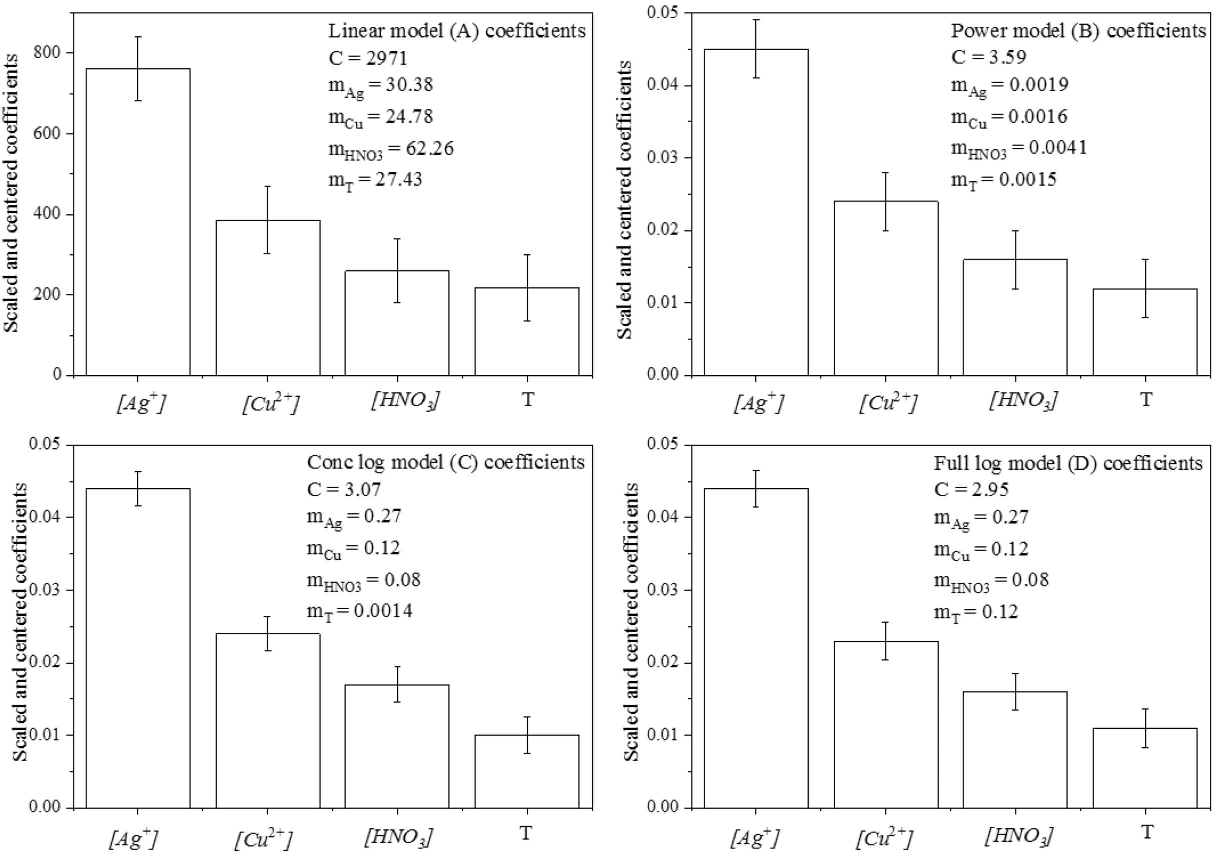
Linear model (A) coefficients
C = 2971
m_{Ag} = 30.38
m_{Cu} = 24.78
m_{HNO3} = 62.26
m_T = 27.43
Scaled and centered coefficients
0
200
400
600
800
$[Ag^+]$
$[Cu^{2+}]$
$[HNO_3]$
T
Power model (B) coefficients
C = 3.59
m_{Ag} = 0.0019
m_{Cu} = 0.0016
m_{HNO3} = 0.0041
m_T = 0.0015
Scaled and centered coefficients
0.00
0.01
0.02
0.03
0.04
0.05
$[Ag^+]$
$[Cu^{2+}]$
$[HNO_3]$
T
Conc log model (C) coefficients
C = 3.07
m_{Ag} = 0.27
m_{Cu} = 0.12
m_{HNO3} = 0.08
m_T = 0.0014
Scaled and centered coefficients
0.00
0.01
0.02
0.03
0.04
0.05
$[Ag^+]$
$[Cu^{2+}]$
$[HNO_3]$
T
Full log model (D) coefficients
C = 2.95
m_{Ag} = 0.27
m_{Cu} = 0.12
m_{HNO3} = 0.08
m_T = 0.12
Scaled and centered coefficients
0.00
0.01
0.02
0.03
0.04
0.05
$[Ag^+]$
$[Cu^{2+}]$
$[HNO_3]$
T

Figure 5

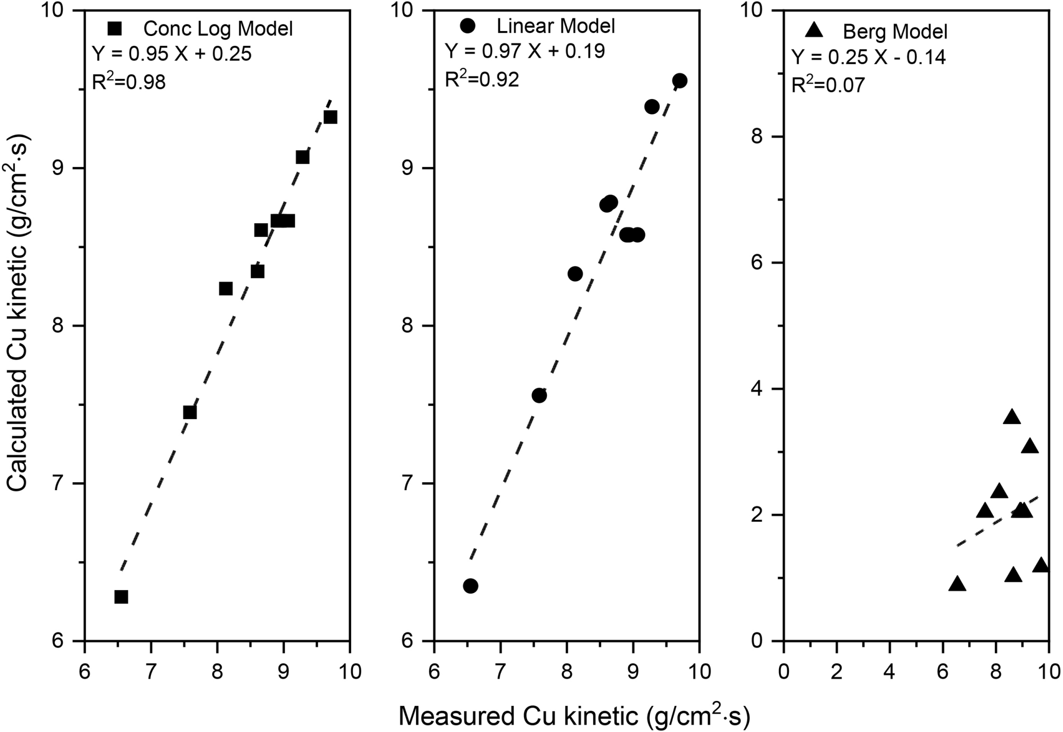
■ Conc Log Model
Y = 0.95 X + 0.25
R^2=0.98
● Linear Model
Y = 0.97 X + 0.19
R^2=0.92
▲ Berg Model
Y = 0.25 X - 0.14
R^2=0.07
Calculated Cu kinetic (g/cm^2·s)
Measured Cu kinetic (g/cm^2·s)
6
7
8
9
10
0
2
4
6
8
10

Figure 6

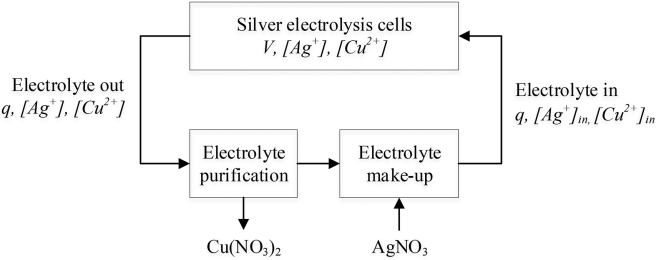
Silver electrolysis cells
$V, [Ag^+], [Cu^{2+}]$
Electrolyte out
$q, [Ag^+], [Cu^{2+}]$
Electrolyte in
$q, [Ag^+]_{in}, [Cu^{2+}]_{in}$
Electrolyte purification
Electrolyte make-up
$Cu(NO_3)_2$
$AgNO_3$

Figure 7

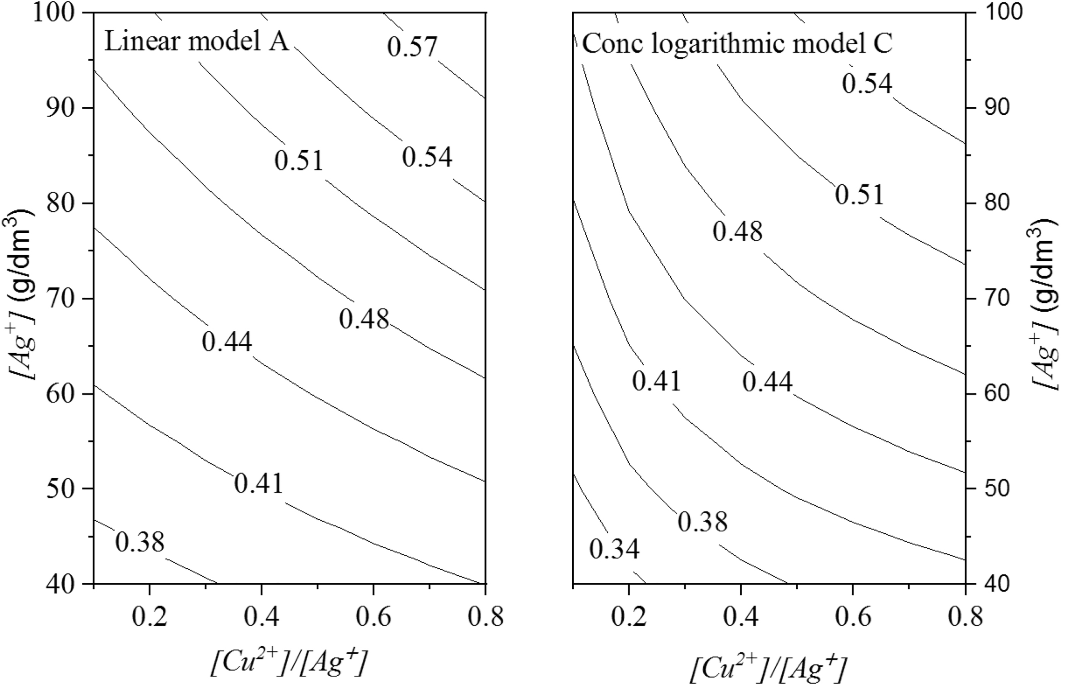
Linear model A
0.57
0.54
0.51
0.48
0.44
0.41
0.38
Conc logarithmic model C
0.54
0.51
0.48
0.44
0.41
0.38
0.34
[Ag+] (g/dm3)
100
90
80
70
60
50
40
0.2
0.4
0.6
0.8
[Cu2+]/[Ag+]

Figure 8

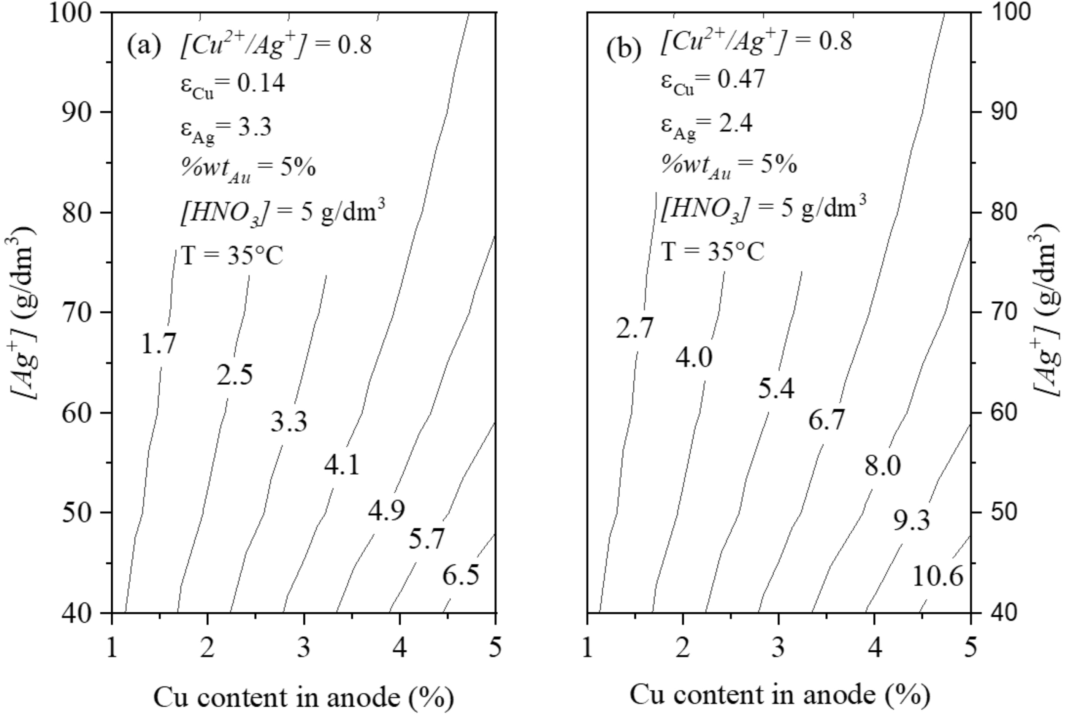
(a) $[Cu^{2+}/Ag^{+}] = 0.8$
$\varepsilon_{Cu} = 0.14$
$\varepsilon_{Ag} = 3.3$
$\%wt_{Au} = 5\%$
$[HNO_3] = 5$ g/dm^3
T = 35°C
1.7
2.5
3.3
4.1
4.9
5.7
6.5
(b) $[Cu^{2+}/Ag^{+}] = 0.8$
$\varepsilon_{Cu} = 0.47$
$\varepsilon_{Ag} = 2.4$
$\%wt_{Au} = 5\%$
$[HNO_3] = 5$ g/dm^3
T = 35°C
2.7
4.0
5.4
6.7
8.0
9.3
10.6
$[Ag^{+}]$ (g/dm^3)
40
50
60
70
80
90
100
Cu content in anode (%)
1
2
3
4
5

Figure 9